Supporting Information

Constructing Sub-10 nm Scale Interfused TiO_2/SiO_x Bi-Continuous Hybrid with Mutual-Stabilizing Effect for Lithium Storage

Ruohan Yu,[1, 2‡] Yexin Pan,[3‡] Yihang Liu,[1‡] Liang Zhou,[1,4] Dongyuan Zhao,[1] Jinsong Wu,[1, 2*] and Liqiang Mai[1, 4*]*

[1]State Key Laboratory of Advanced Technology for Materials Synthesis and Processing, Wuhan University of Technology, Wuhan 430070, P. R. China

[2]Nanostructure Research Centre, Wuhan University of Technology, Wuhan 430070, P. R. China

[3]Division of Integrative Systems and Design, The Hong Kong University of Science and Technology, Clear Water Bay, Kowloon, Hong Kong SAR 999077, P. R. China

[4]Hubei Longzhong Laboratory. Wuhan University of Technology (Xiangyang Demonstration Zone), Xiangyang 441000, Hubei, China

E-mail: liangzhou@whut.edu.cn; wujs@whut.edu.cn; mlq518@whut.edu.cn.

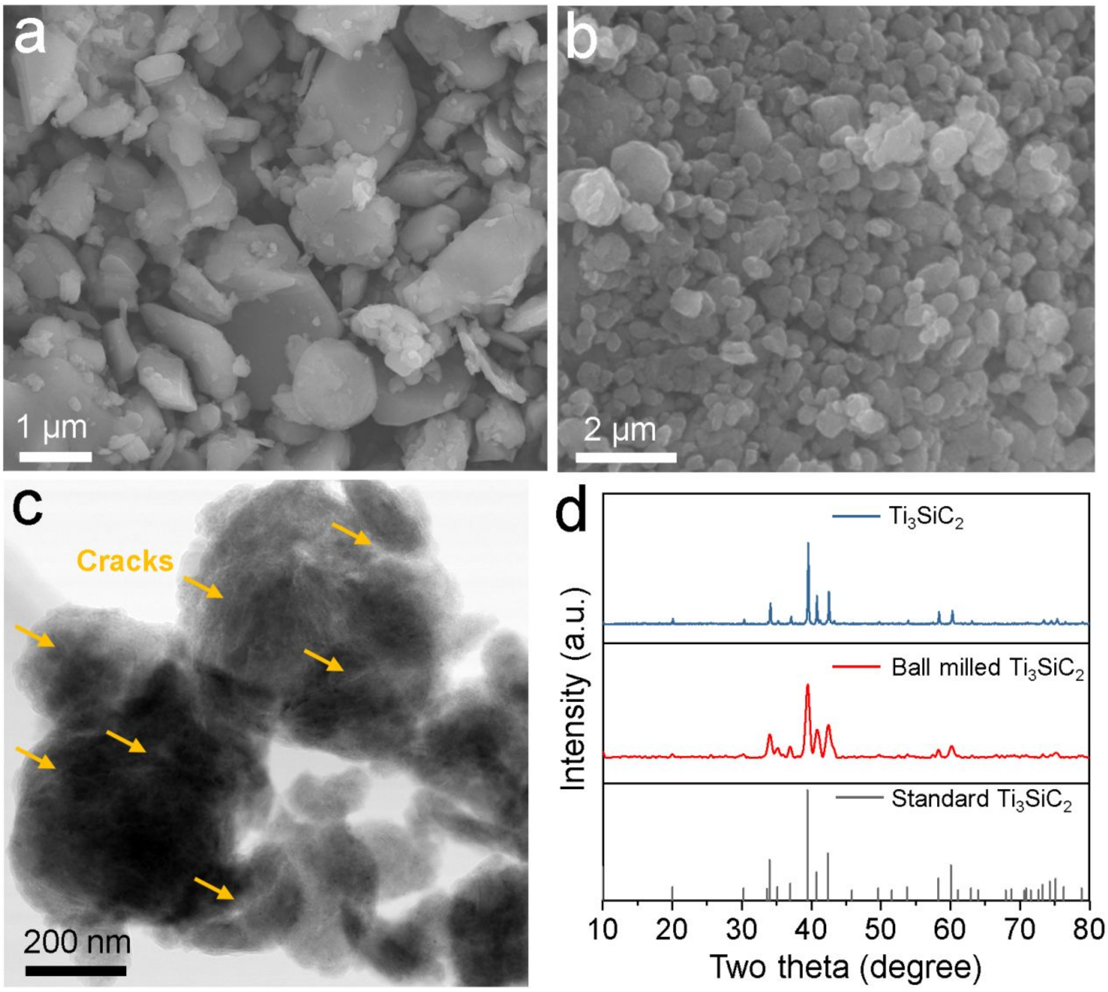

Figure S1. SEM images of the Ti_3SiC_2 before (a) and after (b) ball milling; bright-field STEM image of the Ti_3SiC_2 after ball milling (c); XRD patterns of the Ti_3SiC_2 before and after ball milling (d).

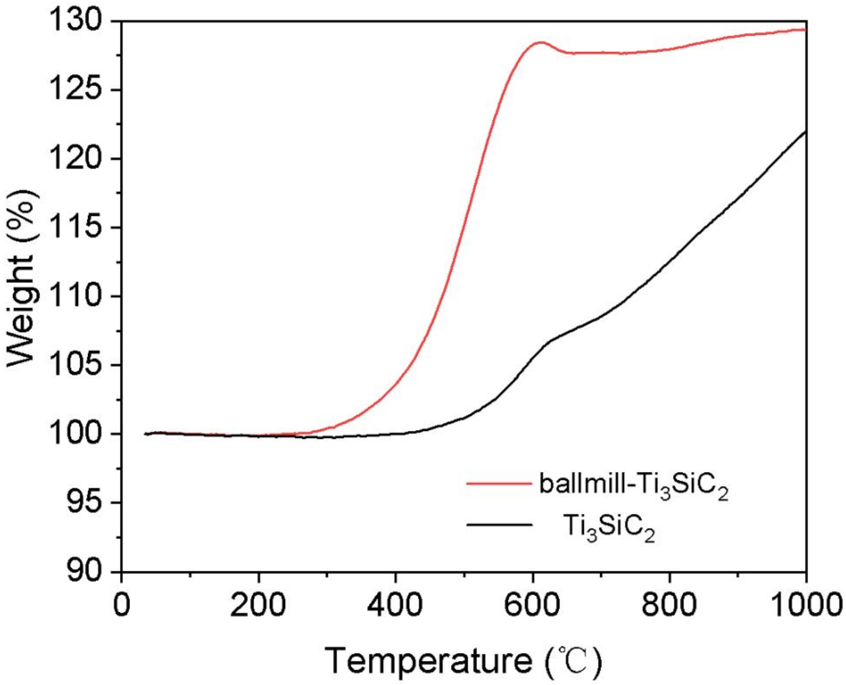

Figure S2. A comparison of TG curves of T_3SiC_2 before and after ball-milling.

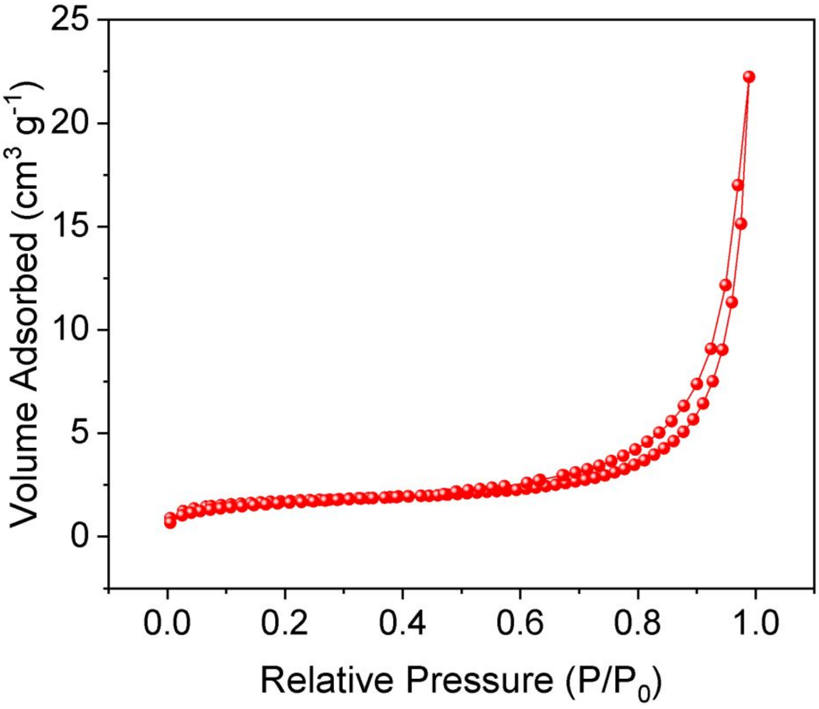

Figure S3. N_2 adsorption–desorption isotherm of the TiO_2/SiO_x hybrid.

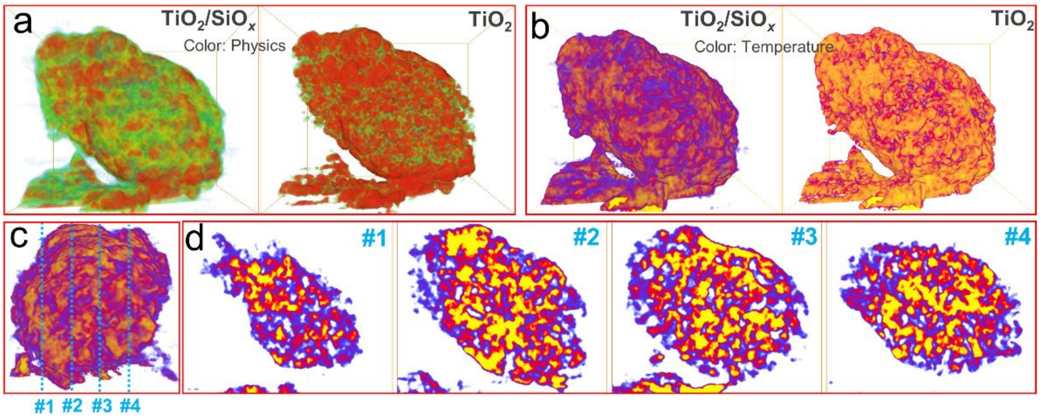

Figure S4. a, Rendered volume using color set "Physics" of TiO_2/SiO_x (left) and TiO_2 only (right) by changing contrast range; **b,** Rendered volume using color set "Temperature" of TiO_2/SiO_x (left) and only TiO_2 (right) by changing contrast range; **c, d,** The right view of the reconstructed particle (c) and representative orthoslices (*xy* planes, perpendicular to the *z* axis at 46, 64, 82 and 100 nm), marked by blue dash line in **c**.

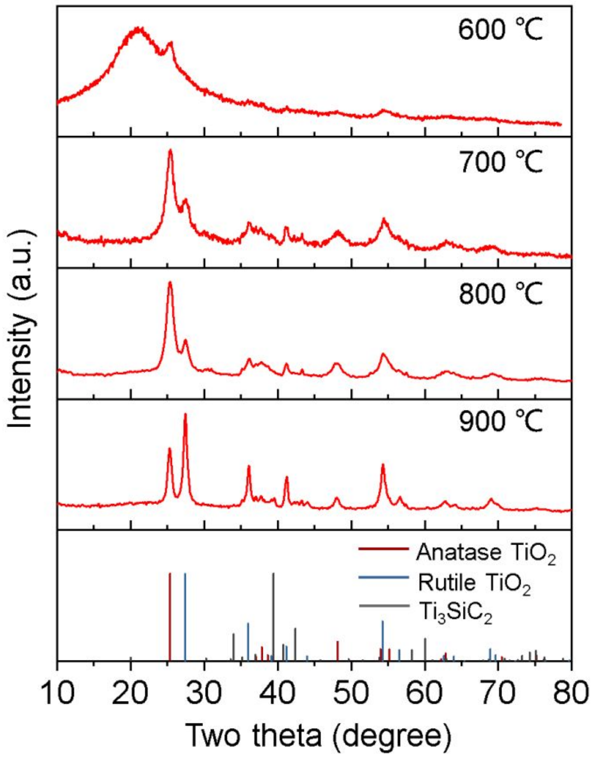

Figure S5. XRD patterns of the TiO_2/SiO_x hybrid prepared at different calcination temperatures.

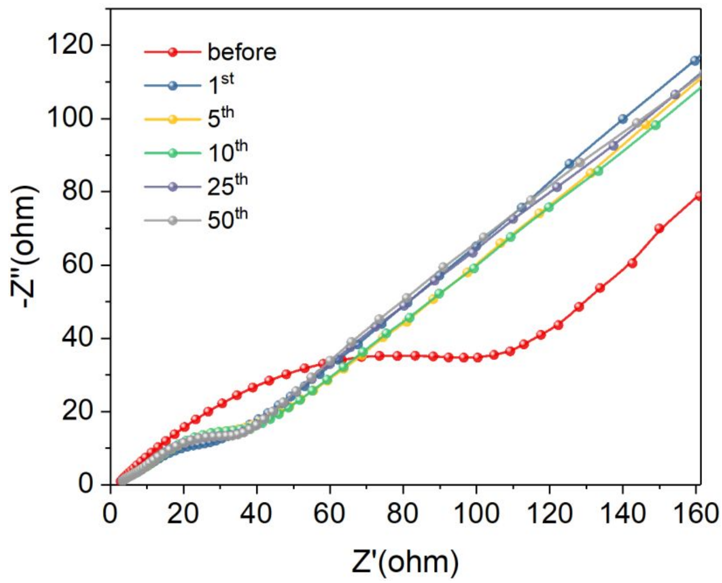

Figure S6. *In-situ* EIS profiles of the TiO_2/SiO_x hybrid electrode before cycling, after 1, 5, 10, 25, and 50 cycles in discharged state.

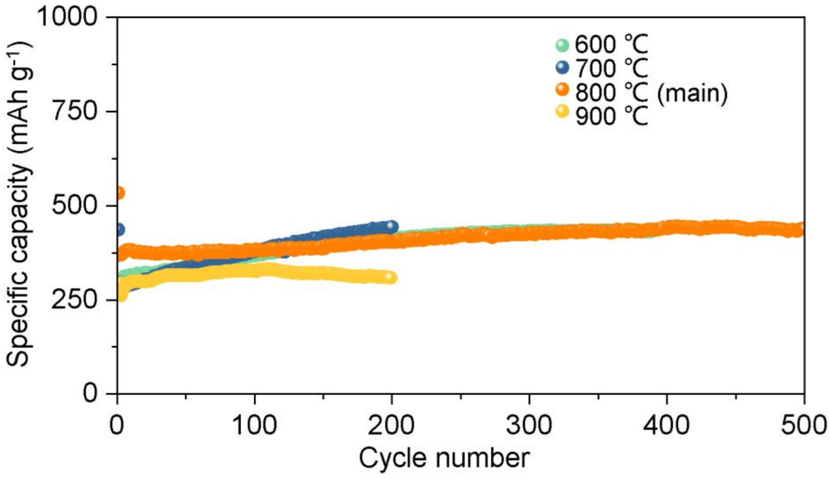

Figure S7. Cycling performances of the TiO_2/SiO_x hybrids prepared at different calcination temperatures at 1.0 A g^{-1}.

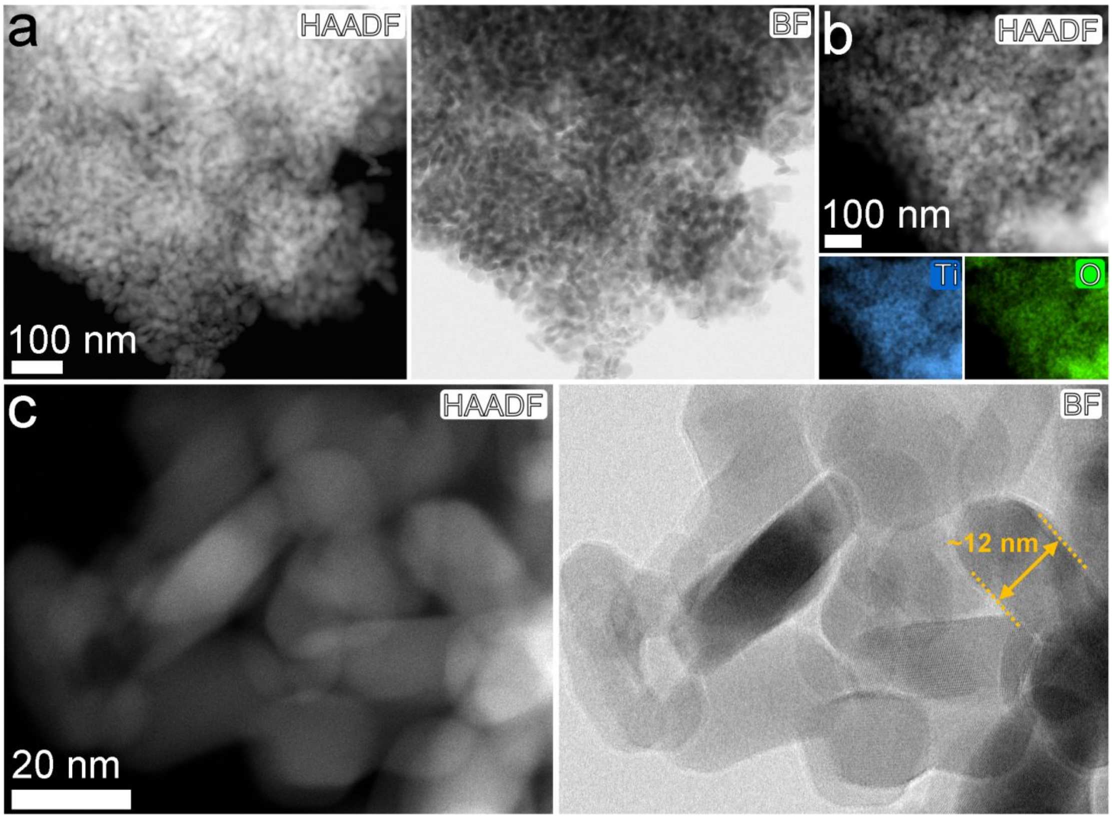

Figure S8. Structural characterization of the anatase TiO_2 nanoparticles. a, HAADF-STEM image and the corresponding BF image; **b,** HAADF image and the corresponding EDX mapping images; **c,** magnified HAADF-STEM image and the corresponding BF image.

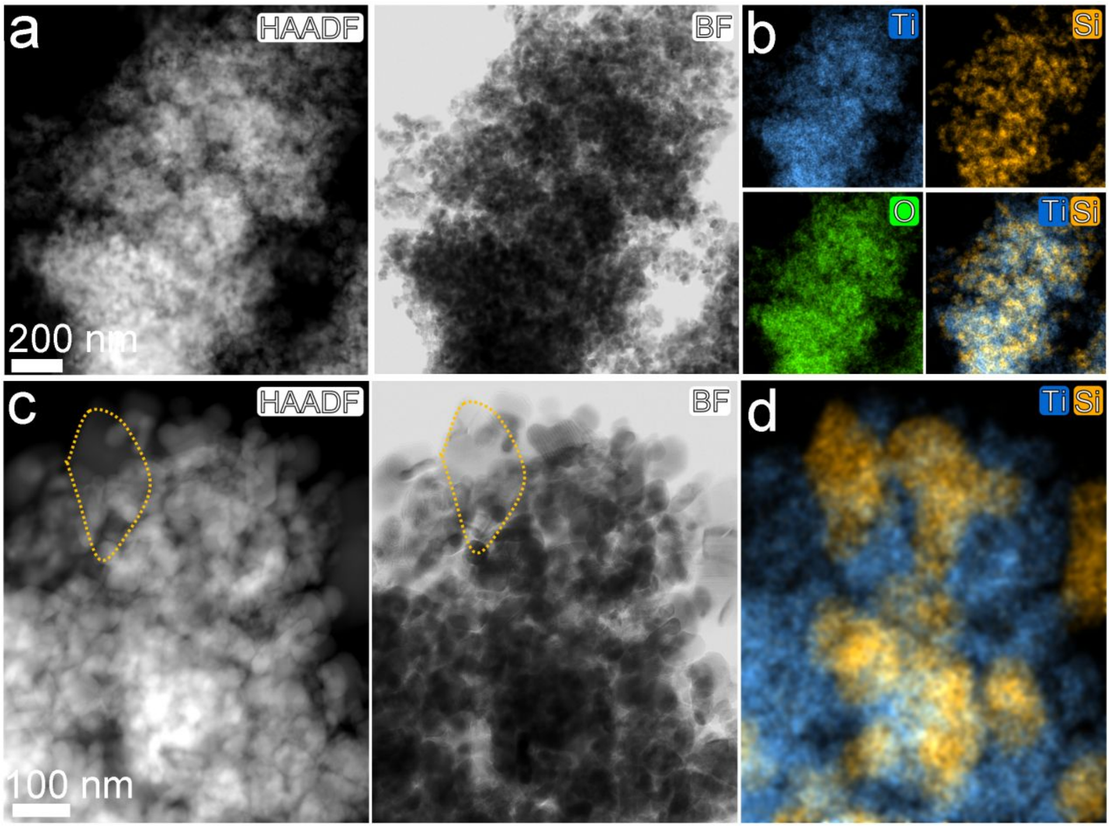

Figure S9. Structural characterization of the mechanically mixed TiO_2/Si mixture. a, HAADF-STEM image and the corresponding BF image; **b,** corresponding EDX images from **a**; **c,** magnified HAADF image and the corresponding BF image; **d,** corresponding EDX mapping color mix image of Si and Ti signals from **c**.

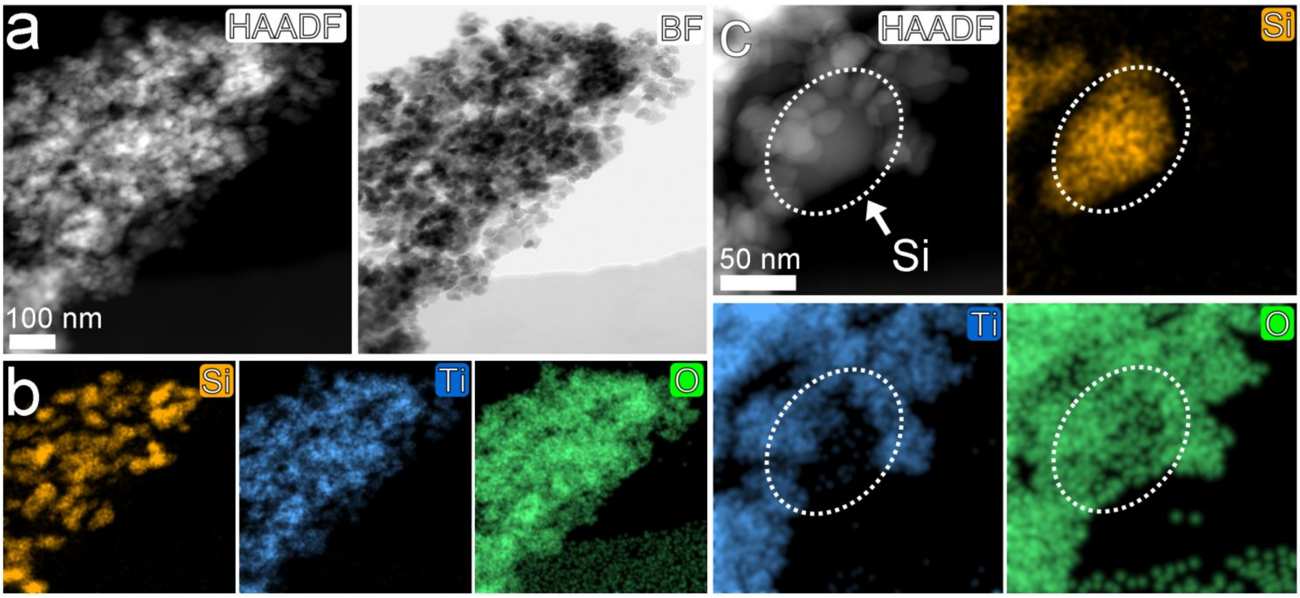

Figure S10. Structural characterization of the mechanically mixed TiO_2/SiO_x mixture. a, HAADF-STEM image and the corresponding BF-STEM image; **b,** corresponding EDX mapping images from **a**; **c,** magnified HAADF-STEM image and corresponding EDX mapping images.

The O signals in (**c**) overlays the Ti and Si signals, indicating that Si nanoparticles are oxidized at the annealing process (800 ^{o}C in air for 2 h).

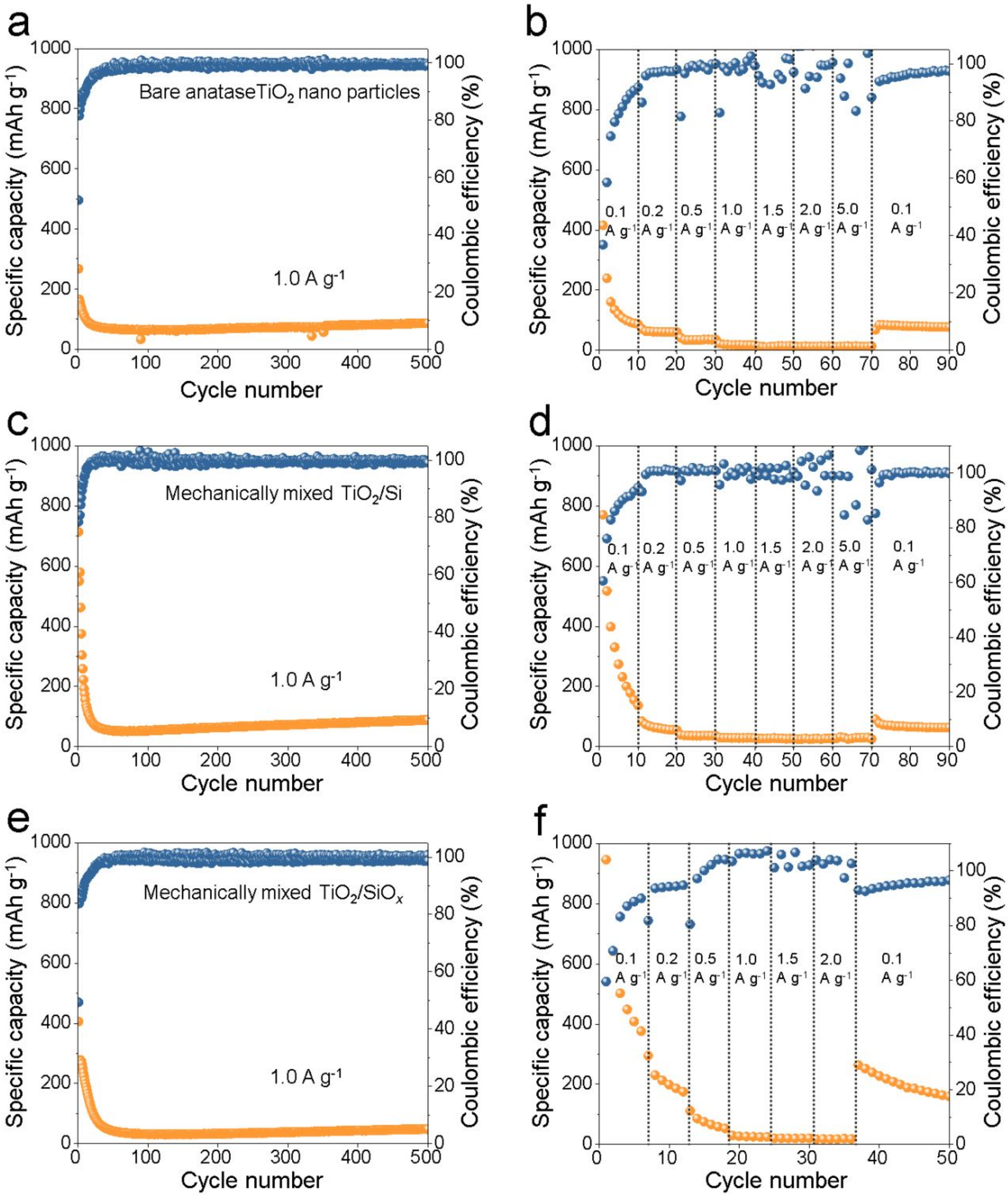

Figure S11. Electrochemical performances of the contrast samples. a, b, Cycling (at 1.0 A g^{-1}) and rate performances of anatase TiO_2 nanoparticles; **c, d,** cycling (at 1.0 A g^{-1}) and rate performances of mechanically mixed TiO_2/Si mixture; **e, f,** cycling (at 1.0 A g^{-1}) and rate performances of mechanically mixed TiO_2/SiO_x mixture.

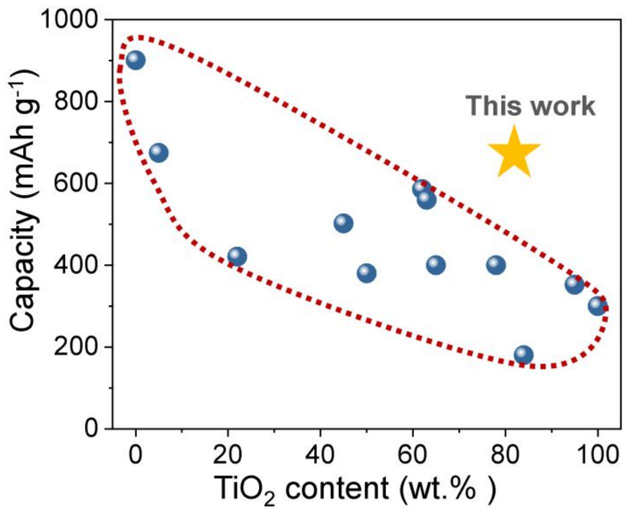

Figure S12. A comparison of retained capacity of various TiO_2 based anode after cycling at a small current density. The statistical data is from Table S1.

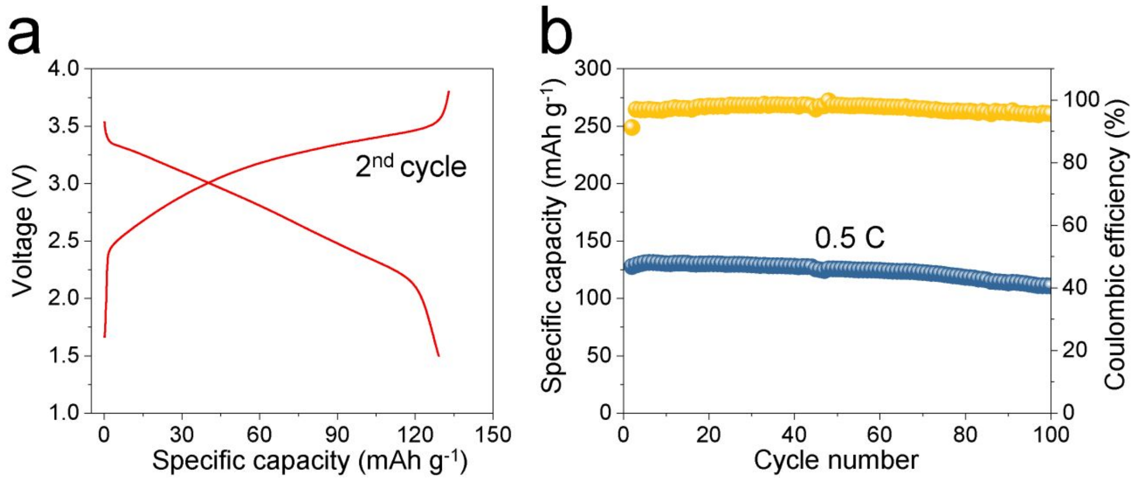

Figure S13. Representative charge–discharge curve (**a**) and cycling performance (**b**) of the $TiO_2/SiO_x//LiFePO_4$ full cell at 0.5 C.

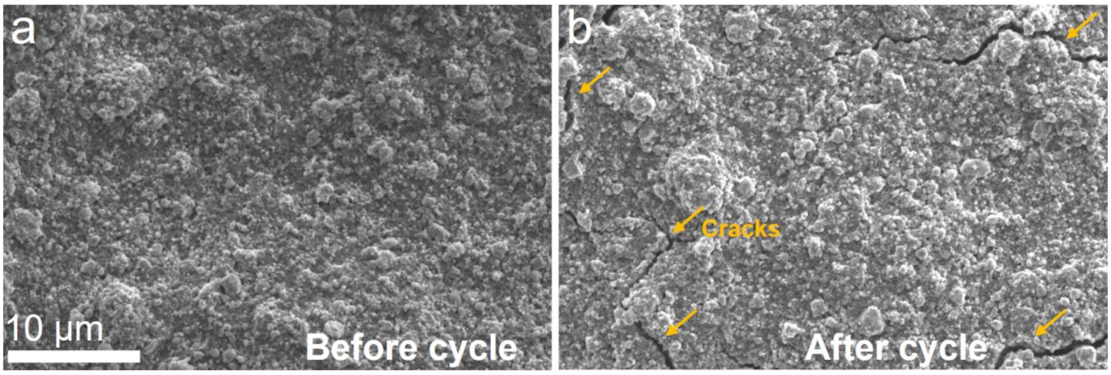

Figure S14. Top-view SEM images of the TiO_2/SiO_x hybrid electrode before (**a**) and after (**b**) cycling.

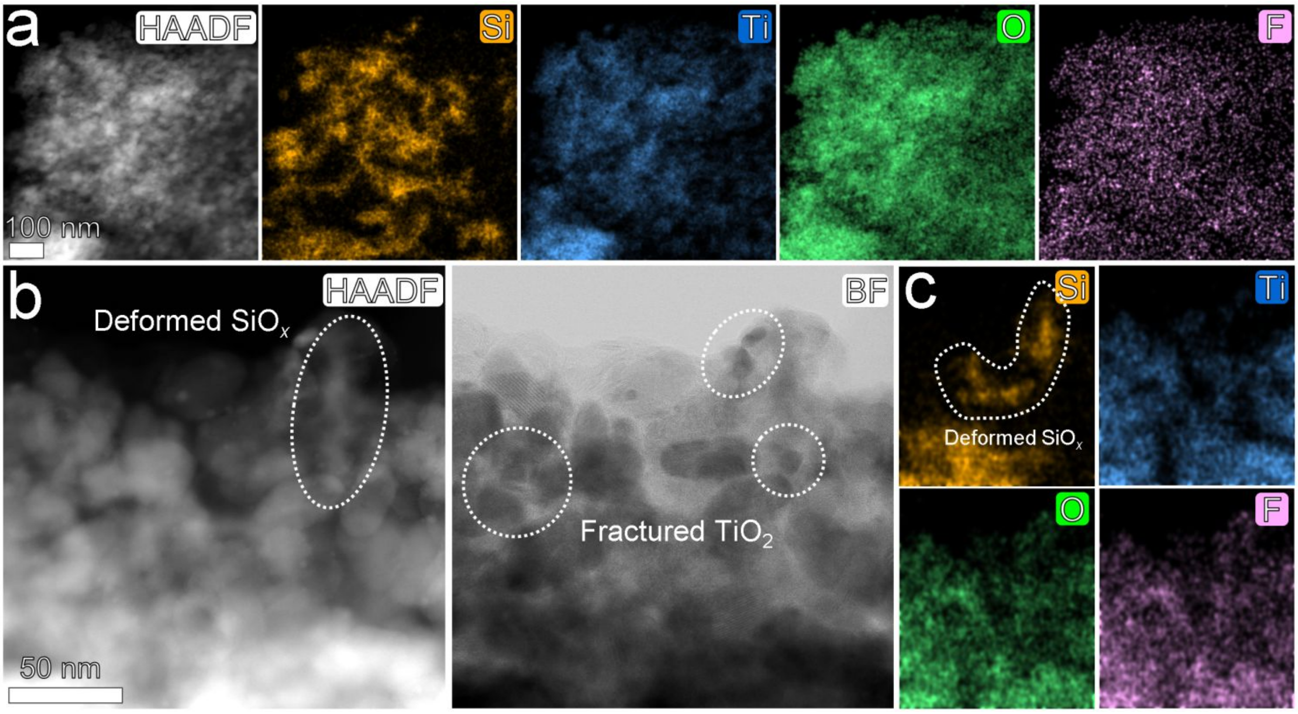

Figure S15. ***Ex-situ*** **characterization of structural degradation of mechanically mixed TiO_2/SiO_x mixture after 500 cycles at 1.0 A g^{-1}. a,** HAADF image and corresponding EDX mapping images of mechanically mixed TiO_2/SiO_x mixture; **b,** magnified HAADF image and the corresponding BF image; **c,** corresponding EDX mapping color mix image of Si and Ti signals from **c**.

It is observed that the SiO_x severely deformed after the cycling process from the Si signal distributions (**a, c**) as well as the marked area in *ex-situ* HAADF image (**b**). Also, the TiO_2 exhibits a fracture and pulverization tendency as observed from the marked areas in *ex-situ* BF image (**b**). These results produce a sharp contrast with the sub-10 nm bi-continuously composited TiO_2/SiO_x hybrid.

Table S1. Electrochemical performances of various TiO_2-based anodes for LIBs.

Materials	Composition ratio(wt.%)	Voltage window	Specific capacity (mAh g^{-1})/Current density (A g^{-1})/Cycle number	Specific capacity (mAh g^{-1})/Current density (A g^{-1})/Cycle number	Rate capacity (mAh g^{-1}) Current density (A g^{-1})	Ref.
TiO_2@SiO_x hybrid	**TiO_2:SiO_x≈82：18**	**0.01-3 V**	**671/0.1/580**	**355/1.0/1000**	**267/5**	**This work**
Anatase TiO_2/RGO	TiO_2:RGO≈95：5	1.0-3.0 V	174/0.17/200	113/1.7/260	88/3.4	[1]
Anatase TiO_2/C	TiO_2:C≈ 84：16	0.01-3.0 V	~180/0.08/100	---	123/0.8	[2]
Anatase TiO_2	TiO_2	0.01-3.0 V	300/0.1/100	242/1.0/1000	220/2.0	[3]
Rutile TiO_2/C	TiO_2:C≈78：21	0-3.0 V	400/0.1/100	140/5.0/10000	172/5	[4]
TiO_2(B)/C	TiO_2:C≈63：37	0.01-3.0 v	560/0.03/100	---	200/0.75	[5]
TiO_2-C/MnO_2	Mainly TiO_2	0.01-3 v	352/0.335/100	218/3.35/150	130/10.05	[6]
TiO_2/SiO_2/C	TiO_2:SiO_2:C≈ 50:35:15	0.01-3 v	380/0.2/700	---	116/8	[7]
C/SiO_x/TiO_2	TiO_2:SiO_2:C≈ 65:21:14	0.01-3 V	400/0.0668/100 200/	---	200/1.67	[8]
TiO_2/SiO_x/C	TiO_2:SiO_x:C≈ 22:40:38	0.005 – 3 V	421/0.067/100	---	---	[9]
SiO@TiO_2	Mainly SiO	0.1 – 3 V	901/0.2/200	---	272/3	[10]
TiO_2-C-SiO	Mainly SiO	0.005 – 2 V	674.5/0.14/100	400/0.7/450	800/1.4	[11]
TiO_2/SiO_2-C	TiO_2:SiO_2:C≈ 45:26:28	0.01 – 3.0 V	502/0.1/300	---	232/2	[12]
TiO_2/SiO_x@C	TiO_2:SiO_x:C≈ 62:21:17	0.01 – 3.0 V	586/0.1/100	365/1/500	401/5	[13]

References

(1) Wang, Z.; Sha, J.; Liu, E.; He, C.; Shi, C.; Li, J.; Zhao, N., A large ultrathin anatase TiO_2 nanosheet/reduced graphene oxide composite with enhanced lithium storage capability. *J. Mater. Chem. A* **2014,** *2* (23), 8893-8901.

(2) Zhang, C.; Zhang, Q.; Kang, S.; Li, X., A novel route for the facile synthesis of hierarchically porous TiO_2/graphitic carbon microspheres for lithium ion batteries. *J. Mater. Chem. A* **2014,** *2* (8), 2801-2806.

(3) He, R.; Liu, Z.; He, P.; Luo, W.; Yu, R.; Hong, X.; Pan, X.; Zhou, Q.; Mai, L.; Zhou, L., Constructing three-dimensional macroporous TiO_2 microspheres with enhanced pseudocapacitive lithium storage under deep discharging/charging conditions. *ACS Appl. Mater. Interfaces* **2021,** *13* (14), 16528-16535.

(4) Wang, P.; Lang, J.; Liu, D.; Yan, X., TiO_2 embedded in carbon submicron-tablets: synthesis from a metal–organic framework precursor and application as a superior anode in lithium-ion batteries. *Chem. Commun.* **2015,** *51* (57), 11370-11373.

(5) Yang, Z.; Du, G.; Guo, Z.; Yu, X.; Chen, Z.; Guo, T.; Liu, H., TiO_2(B)@carbon composite nanowires as anode for lithium ion batteries with enhanced reversible capacity and cyclic performance. *J. Mater. Chem.* **2011,** *21* (24), 8591-8596.

(6) Liao, J.-Y.; Higgins, D.; Lui, G.; Chabot, V.; Xiao, X.; Chen, Z., Multifunctional TiO_2–C/MnO_2 core–double-shell nanowire arrays as high-performance 3D electrodes for lithium ion batteries. *Nano Lett.* **2013,** *13* (11), 5467-5473.

(7) Jiang, Y.; Chen, S.; Mu, D.; Zhao, Z.; Li, C.; Ding, Z.; Xie, C.; Wu, F., Flexible TiO_2/SiO_2/C film anodes for lithium-ion batteries. *ChemSusChem* **2018,** *11* (13), 2040-2044.

(8) Yang, Z.; Ding, Y.; Jiang, Y.; Zhang, P.; Jin, H., Hierarchical C/SiO_x/TiO_2 ultrathin nanobelts as anode materials for advanced lithium ion batteries. *Nanotechnology* **2018,** *29* (40), 405602.

(9) Wang, X.; Xia, Y.; Zuo, X.; Schaper, S. J.; Yin, S.; Ji, Q.; Liang, S.; Yang, Z.; Xia, S.; Xiao, Y., Synergistic effects from super-small sized TiO_2 and SiO_x nanoparticles within TiO_2/SiO_x/carbon nanohybrid lithium-ion battery anode. *Ceram. Int.* **2019,** *45* (11), 14327-14337.

(10) Xu, D.; Chen, W.; Luo, Y.; Wei, H.; Yang, C.; Cai, X.; Fang, Y.; Yu, X., Amorphous TiO_2 layer on silicon monoxide nanoparticles as stable and scalable core-shell anode materials for high performance lithium ion batteries. *Appl. Surf. Sci.* **2019,** *479*, 980-988.

(11) Dou, F.; Shi, L.; Song, P.; Chen, G.; An, J.; Liu, H.; Zhang, D., Design of orderly carbon coatings for SiO anodes promoted by TiO_2 toward high performance lithium-ion battery. *Chem. Eng. J.* **2018,** *338*, 488-495.

(12) Liu, H.; Wolf, M.; Karki, K.; Yu, Y.-S.; Stach, E. A.; Cabana, J.; Chapman, K. W.; Chupas, P. J., Intergranular cracking as a major cause of long-term capacity fading of layered cathodes. *Nano Lett.* **2017,** *17* (6), 3452-3457.

(13) Shi, W.; Meng, J.; Li, Q.; Xiao, Z.; Xu, X.; Qin, M.; Zhang, X.; Mai, L., Ternary TiO_2/SiO_x@ C nanocomposite derived from a novel titanium–silicon MOF for high-capacity and stable lithium storage. *Chem. Commun.* **2020,** *56* (18), 2751-2754.